#### Research Article

Syed Muhammad Raza Shah Naqvi, Umair Manzoor, Hassan Waqas, Dong Liu\*, Hamzah Naeem, Sayed M. Eldin, and Taseer Muhammad

# Numerical investigation of thermal radiation with entropy generation effects in hybrid nanofluid flow over a shrinking/stretching sheet

https://doi.org/10.1515/ntrev-2023-0171 received June 4, 2023; accepted November 23, 2023

Abstract: The need for efficiency in nanotechnology has spurred extraordinary development. Hybrid nanofluids, which are base fluids injected with nanoparticles, have a great potential for thermal enhancement in thermal systems. Particularly promising for magnetic thermal engineering are magnetic hybrid nanofluids. Understanding dynamic transport in Graphene Oxide (GO)-Fe<sub>3</sub>O<sub>4</sub>/H<sub>2</sub>O and GO/H<sub>2</sub>O nanofluids over stretching and shrinking surfaces, with severe entropy consequences, is still uncharted territory. To fully grasp this complexity, our study examines the numerical investigation of entropy formation in magnetohydrodynamic (MHD) hybrid nanofluids. The aim of this study is to establish a mathematical framework for understanding entropy production in the context of MHD, unsteady, incompressible flow of hybrid nanofluid flow over surfaces that experience both stretching and shrinking. The investigation encompasses the influence of MHD effects and nonlinear thermal radiation on flow behavior. The governing modeled form is modified into solvable representations in Cartesian configuration and then addressed utilizing the built-in bvp4c approach in MATLAB. For numerous quantities of the relevant parameters, several key features of flow and heat transmission are explored, discussed, and illustrated utilizing tables and graphs. Furthermore, the heat transfer properties in a magnetic field have been improved dramatically. The comprehensive entropy generation rate was condensed by up to 41% as opposed to refined water, according to the findings from the analysis.

**Keywords:** magnetohydrodynamics, hybrid nanofluid, entropy generation, thermal radiation, MATLAB

#### Nomenclature

space-dependent coefficient a,bconstants temperature-dependent coefficient В Brinkman number Br strength of magnetic field (T) skin friction coefficient  $C_{\mathrm{f}}$ strength of electric field (N/C)  $E_0$ electric field parameter  $E_1$ acceleration due to gravity (m s<sup>-2</sup>)

magnetic field parameter M Nu Nusselt number

shape factor P fluid pressure (Pa) Prandtl number Pr

radiative heat flux (W m<sup>-2</sup>)

Reynolds number Re radiation parameter Rd S suction/injection T fluid temperature (K)  $T_{\rm w}$ surface temperature (K)

free stream temperature (K)

velocity component (m s<sup>-1</sup>) u,v

wall mass transfer

#### \* Corresponding author: Dong Liu, School of Energy and Power Engineering, Jiangsu University, Zhenjiang 212013, China, e-mail: liudong@ujs.edu.cn

Syed Muhammad Raza Shah Naqvi, Hassan Waqas: School of Energy and Power Engineering, Jiangsu University, Zhenjiang 212013, China Umair Manzoor, Hamzah Naeem: Department of Mathematics, Government College University, Layyah Campus 31200, Faisalabad, **Pakistan** 

Sayed M. Eldin: Center of Research, Faculty of Engineering, Future University in Egypt, New Cairo 11835, Egypt

Taseer Muhammad: Department of Mathematics, College of Sciences, King Khalid University, Abha 61413, Saudi Arabia

# **Greek symbols**

- thermal expansion (K<sup>-1</sup>)
- density (kg m<sup>-3</sup>) ρ

Ω dimensionless temperature ratio δ unsteadiness parameter heat capacity (J kg<sup>-1</sup> K<sup>-1</sup>)  $c_{\rm p}$ δ unsteadiness parameter dynamic viscosity (kg m<sup>-1</sup> s<sup>-1</sup>) μ Stefan-Boltzmann constant (W m<sup>-2</sup> K<sup>-4</sup>)  $\sigma^*$ λ mixed convection parameter σ electric conductivity (S m<sup>-1</sup>) kinematic viscosity (m<sup>2</sup> s<sup>-1</sup>) υ thermal conductivity (W m<sup>-1</sup> K<sup>-1</sup>) κ

## **Subscripts**

 $s_2$ 

f base fluid nf nanofluid hnf hybrid nanofluid first solid nanoparticle  $S_1$ second nanoparticle

### 1 Introduction

Now, scientists are deeply involved in their investigation of nanotechnology. Numerous heat transfer technologies are extensively used in industry, which has also sped up the development of applications that deal with energy. Transportation, manufacturing, and other basic functions that are closely related to heat exchange processes, such as heating food and materials, have all undergone tremendous technological advancement. For improving thermal performance in this environment, nanofluids have become an appealing choice of Kleinstreuer and Xu [1]. The innovative work of Choi and Eastman [2] showed the mastery of nanofluids for cooling purposes in a variety of technological applications. The fact that nanofluids differ from traditional base fluids in their ability to transport heat is noteworthy and suggests that the field of thermal enhancement may be about to undergo a revolution. Hybrid nanofluids are defined as mixtures in which different nanoparticles with different chemical properties are incorporated into a base fluid to enhance the thermal efficiency of nanofluids.

Esfe et al. [3] introduced how to enhance the efficiency of the heat transfer rate of nanofluid by utilizing the MgOwater in order to reduce the cost. For the optimization of nanoparticles Response surface method (RSM) is used to attain the cost function and heat transfer coefficient function. On the basis of different thermo physical properties, Sharma et al. [4] investigated the metamodel framework to

predict the effects of nanoparticles concentration and the temperature of nanofluid.

Mahian et al. [5] introduced the applications of nanofluid in wide ranges including the renewable energy system, also discussed the positive impact of the energy systems with the environmental point of view by using nanofluid.

These fluids are employed in several engineering and industrial applications, including heat exchangers, solar cells, solar collectors [6], heating conduits, cooling systems, and coolants for machinery and production processes [7]. Additionally, they work in the biomedical sector, auto production, maritime operations, nuclear system cooling, and refrigeration system cooling. Shojaie Chahregh and Dinarvand [8] worked on the applications of the nanofluid in the drug delivery through artery by using TiO2 and Ag over a porous channel. Saleh et al. [9] introduced the differential transformation method to describe the convective boundary on heat transfer analysis using carbon nanotubes incorporated with magnetic field with suction/injection phenomenon. Ahmad et al. [10] worked on magnetohydrodynamic (MHD) flow of nanofluid flow by using metallic nanoparticles taking blood as a base fluid. The new thermal and magnetic properties of two different types of hybrid nanofluid graphene oxide (GO)-Fe<sub>3</sub>O<sub>4</sub>/engine oil (EO) and mono nanofluid GO/EO were studied by Ahmad et al. [11] (Table 1). The effects of both induced and applied magnetic fields were considered in this study. In order to analyze the flow behavior of a hybrid nanofluid through a permeable Darcy porous medium, Abu Bakar et al. [12] investigated the slip effects with radiation over a shrinking sheet. Zainal et al. [13] performed a monetary analysis that investigated hybrid Al<sub>2</sub>O<sub>3</sub>-Cu/H<sub>2</sub>O nanofluid flow towards a permeable stretching/shrinking sheet, and its MHD behavior, considering the presence of quadratic velocity effects. In recent years, researchers have conducted various additional studies focusing on hybrid nanofluids. Neethu et al. [14] used TiO with Ag in water over a sheet with suction, Mahesh et al. [15] contemplated same hybrid nanoparticles in water over porous sheet, Devi and Devi [16] took into account copper and aluminum oxide in water on the same geometry, and the same geometry and same hybrid particles were studied by Venkateswarlu and Satya Narayana [17] along with viscous dissipation.

Temperature distribution changes under the influence of thermal emissions, specifically in flows which undergo the chemical reactions. The re-entry of spacecraft, astrophysical flows, the production of electricity, and solar power technology are a few examples of varied situations where this effect is relevant [18]. A lot of investigation into the effects of radiative and thermal control in nanofluids has been done over the years. By taking into account the

Table 1: Physical properties of the base fluid (water) and nanoparticles GO and Fe<sub>3</sub>O<sub>4</sub> [11]

Physical properties	$\rho$ (kg/m <sup>3</sup> )	$C_{\rm p}$ (J/kgK)	k (W/mK)	$\beta \times 10^5 (\text{K}^{-1})$
Fluid (water)	997.1	4,179	0.613	21
	1,800	717	5,000	0.284
GO	5,180	670	9.7	$0.74 \times 10^{6}$
Fe <sub>3</sub> O <sub>4</sub>				

combined effects of permeable moving surface under the influence of MHD and heat radiation, Zainal et al. [19] explored the flow and heat allocation dynamics of a hybrid nanofluid (Cu-Al<sub>2</sub>O<sub>3</sub>/water). Unsteady MHD hybrid nanofluid flow across a stretched surface was used to study the movement of heat and mass by Sreedevi et al. [20]. This experiment included thermal radiation, chemical reactions, suction, and slide effects. In a study, Mabood et al. [21] explained the different physical properties of a hybrid water-based nanofluid under the effects of thermal radiation. Many scientists have recently investigated how thermal radiation affects the dynamics of heat transfer inside the flow of hybrid nanofluids. Shatnawi et al. [22] studied the effects of nonlinear radiation on hybrid nanofluid flow of Casson fluid along with magnetic effects. In another study, thermal radiation effects on hybrid nanofluid flow over a Riga sheet were explored by Shatwani et al. [23]. Entropy generation occurs throughout a range of thermal processes and is linked to thermodynamic irreversibility. Entropy heat production is caused by numerous types of irreversibility, including heat flow along a thermal profile, features of laminar thermal transmission, and the viscosity reaction. Engineering perspectives include emphasizing irreversibility and seeking components that promote entropy generation, as entropy is linked to a measure of disorder that reduces the performance of thermal systems. Entropy analysis is presently being used in a variety of applications, spinning reactors, heat exchangers, nuclear fuel rod cooling, and solar energy collectors are a few examples of these industries. Total entropy rate on a convectively heat disk was calculated by Khan et al. [24] while considering the effects of magnetic field and ohmic dissipation. Entropy generation of boundary layer hybrid nanofluid flow under the effects of magnetic field and thermal radiation was discussed by Seth et al. [25]. Sithole et al. [26] provided an insight into entropy generation of nanofluid flow over heated sheet under the influence of viscous dissipation and thermal

radiation. Fatunmbi and Salawu [27] talked about micropolar nanofluid flow induced by chemical reaction, mass flux, and multiple slip. They provided an insight into entropy calculations of this type of flow. Entropy generation of Brownian motion and thermophoresis effects on non-Newtonian nanofluid over stretching sheet was calculated by Bhatti et al. [28]. Hayat et al. [29] also calculated the entropy generation of nonlinear mixed convection of tangent hyperbolic nanomaterials.

## 2 Novelty

Motivated by the preceding research, the current work intends to examine the implications of thermal radiation on hybrid nanoliquid GO-Fe<sub>3</sub>O<sub>4</sub>/H<sub>2</sub>O flow across a linear stretching/shrinking surface using Tiwari and Das's [30] nanofluid model. This framework examines the repercussions of hybrid nanofluid while taking GO and Fe<sub>3</sub>O<sub>4</sub> nanomaterials into consideration. The similarity approach reduces the transport problem's primary equations to ordinary differential equations (ODEs). The nonlinear ODEs were numerically employed in the MATLAB built-in bvp4c method. To corroborate the obtained numerical outcome, it was compared to prior research in the literature. There is no prior record of this precise merger.

- 1) We take into account a factor that has not been fully covered in other studies: the simultaneous impact of both electric and magnetic fields.
- Our investigation covers the properties of two different kinds of nanofluids: GO/H2O designated as a mono nanofluid, and GO-Fe<sub>3</sub>O<sub>4</sub>/H<sub>2</sub>O, designated as a hybrid nanofluid.
- 3) We explore the effects of suction, chemical reaction, non-uniform heat flux, and activation energy in both types of nanofluids, enhancing our knowledge of these factors' functions.

The findings of this research offer excellent promise for number of useful applications. These improved potentials of hybrid nanofluids will be used to greatly boost heat exchanger efficiency and energy savings, revolutionizing the field of thermal engineering. These nanofluids may provide accurate temperature control and effective heat transmission in the field of magnetic thermal engineering, having an impact on industries like electronics cooling and medical treatments that require regulated localized heating. Improved cooling systems and better material processing could assist industries including automotive, aerospace, and manufacturing, and the lower entropy generation could lead to more environmentally friendly procedures. The study's ramifications also cover energy conversion, advances in nanotechnology, and even the use of renewable energy sources, displaying a wide range of real-world uses.

### 2.1 Physical description of the model

The fluid passes with wall velocity  $u_{\rm w}(x,t)$  over the sheet that shifts over time extemporaneously stretched from opposite sides. The orientation of the Cartesian coordinates is set such that flow is restricted in the zone where the x-axis is parallel to the surface and the y-axis is assumed to be perpendicular to it, as shown in Figure 1.

The following assumptions are included in this framework:

- The flow is presumed to be unsteady, 2-dimensional, and incompressible.
- Both electric and magnetic fields are provoked orthogonal to the fluid flow.
- The wall temperature is indicated by  $T_{\rm w}$  and the free stream temperature by  $T_{\infty}$  that is less than the wall temperature.

### 2.2 Mathematical modeling

The leading equations are as follows [31]:

$$u_x + v_y = 0, (1)$$

where u and v are velocity components along the x, y axes.

$$u_t + uu_x + vu_y = -\frac{1}{\rho_{\text{hnf}}} P_x + v_{\text{hnf}} (u_{xx} + u_{yy})$$

$$+ \frac{\sigma_{\text{hnf}}}{\rho_{\text{hnf}}} (EB - B^2 u)$$

$$+ \frac{(\rho \beta)_{\text{hnf}}}{\rho_{\text{hnf}}} (T - T_{\infty}) g,$$
(2)

where P denotes the pressure of the fluid,  $\rho_{\rm hnf}$  is the density of the hybrid fluid,  $v_{\rm hnf}$  is the kinematic viscosity, g is the gravity,  $\sigma_{\rm hnf}$  is the electric conductivity, temperature of the fluid and free stream temperature are denoted as  $T \& T_{\infty}$ , E is the electric field, and B is temperature-dependent coefficient.

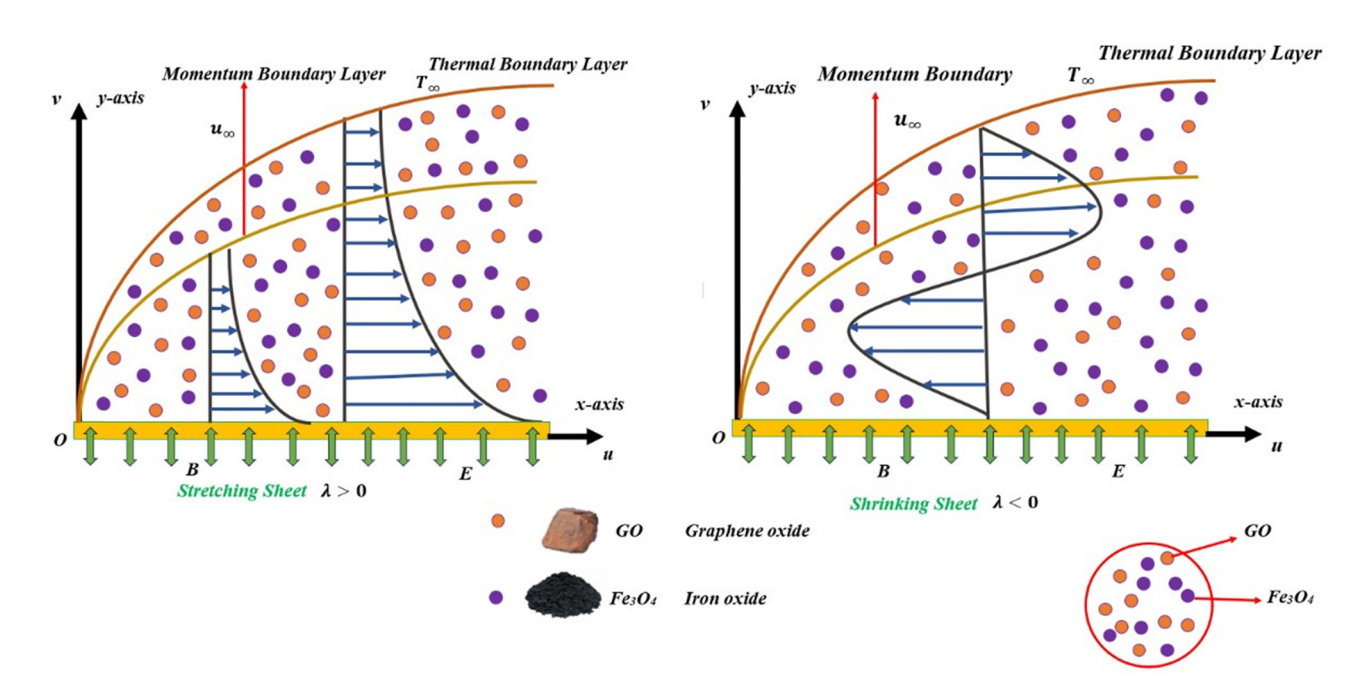


Figure 1: Flow geometry of the problem.

$$v_t + uv_x + vv_y = -\frac{1}{\rho_{\text{bnf}}} P_y + v_{\text{hnf}} (v_{xx} + v_{yy}),$$
 (3)

$$T_{t} + uT_{x} + vT_{y} = \alpha_{hnf}(T_{xx} + T_{yy}) - \frac{1}{(\rho c_{p})_{hnf}}(q_{r})_{y} + \frac{q'''}{(\rho c_{p})_{hnf}} + \frac{\mu_{hnf}(2((u_{x})^{2} + (v_{y})^{2}) + (u_{y} + v_{x})^{2})}{(\rho c_{p})_{hnf}} + \frac{\mu_{hnf}}{(\rho c_{p})_{hnf}}(u_{y})^{2}$$
(4)

where radiative heat flux and heat generation/absorption are given as  $q_{\rm r}$  &  $q^{\prime\prime\prime}$ , heat capacity and dynamic viscosity of the hybrid nanofluid are denoted by  $c_{\rm p}$  &  $\mu_{\rm hnf}$ , respectively.

#### 2.3 Governing boundary constraints

The subjected boundary conditions are [31,32] as follows:

$$u = u_{w}(x, t), v = v_{w}(x, t), T = T_{w}(x, t), |_{at y=0}$$

$$u \to 0, T \to T_{\infty}|_{as y \to \infty}$$
(5)

where  $u_w = \frac{c}{1 - at}x$  signify the linear shrinking sheet velocity and  $v_w$  symbolizes the mass transfer at the wall.

Variable heat generation/absorption is represented by q''' in equation (4).

$$q''' = \frac{k_{\rm hnf}}{v_{\rm hnf}} \left[ \frac{\bar{A}(T_{\rm w} - T_{\infty})u_{\rm w}(x, t)f' + \bar{B}k_{\rm hnf}u_{\rm w}(x, t)(T - T_{\infty})}{x} \right]. \tag{6}$$

According to the Rosseland technique, the condition (A, B) > 0 in this case denotes heat generation within the flow, while (A, B) < 0 denotes heat absorption from the flow.

$$q_{\rm r} = -\frac{4\sigma^*}{3k^*}(T^4)_{\rm y},\tag{7}$$

where  $k^*$  is the mean absorption coefficient and  $\sigma^*$  designates the Stefan–Boltzmann coefficient. Using Taylor's expansion of  $T^4$  about T, we obtain while neglecting terms with higher order.

$$T^2 \cong 4T_{\infty}^3 T - 3T_{\infty}^4. \tag{8}$$

Adding equation (7) with equation (4) yields the following:

$$(\rho c_{\rm p})_{\rm hnf}(T_{\rm t} + uT_{\rm x} + vT_{\rm y}) = k_{\rm hnf}(T_{\rm xx} + T_{\rm yy}) + \frac{16T_{\infty}^3}{3k^*}T_{\rm yy} + \mu_{\rm hnf}(u_{\rm y})^2 + q'''.$$
(9)

Engaging the boundary layer estimation as

$$u \gg v,$$

$$u_{y} \gg u_{x}, v_{t}, v_{x}, v_{y},$$

$$T_{y} \gg T_{x},$$

$$P_{y} = 0.$$
(10)

After the execution of equation (10) in equations (2)–(4), we obtained the following expressions:

$$u_x + v_y = 0, \tag{11}$$

$$u_{t} + uu_{x} + vu_{y} = v_{hnf}(u_{yy}) + \frac{\sigma_{hnf}}{\rho_{hnf}}(EB - B^{2}u) + \frac{(\rho\beta)_{hnf}}{\rho_{hnf}}(T - T_{\infty})g,$$
(12)

$$T_{t} + uT_{x} + vT_{y} = \alpha_{hnf}(T_{yy}) + \frac{1}{(\rho c_{p})_{hnf}} \left[ \frac{16T_{\infty}^{3}\sigma^{*}}{3k^{*}} T_{yy} \right] + \frac{Q_{0}(T - T_{\infty})}{(\rho C_{n})_{hnf}} + \mu_{hnf}(u_{y})^{2}.$$
(13)

#### 2.4 Similarity formulation [31,32]

$$\psi = \sqrt{\frac{bv_{f}}{1 - at}} x f(\zeta), \ \zeta = y \sqrt{\frac{b}{(1 - at)v_{f}}},$$

$$T_{w} = \frac{bxT_{0}}{2v_{f}(1 - at)^{2}} + T_{\infty}, \theta = \frac{T - T_{\infty}}{T_{w} - T_{\infty}}.$$
(14)

The stream function of the flow problem is designated as

$$u = \psi_y, \quad v = -\psi_x. \tag{15}$$

#### 2.5 Modified flow model

After the implementation of similarity formulation, equations (11)–(13) get the following form:

$$A_{1}f'''(\zeta) + A_{2}\left[ff''(\zeta) - (f'(\zeta))^{2} - \left[f'(\zeta) + \frac{\zeta}{2}f''(\zeta)\right]\delta\right] + A_{3}M(E_{1} - f'(\zeta)) + A_{4}\lambda^{*}\theta,$$
(16)

$$\left(A_5 + \frac{4}{3} \operatorname{Rd}\right) \theta''(\zeta) + A_6 \operatorname{Pr} \left[\theta'(\zeta) f(\zeta) - f'(\zeta) \theta(\zeta) - \delta \left(\frac{\zeta}{2} \theta'(\zeta) + 2\theta(\zeta)\right)\right] + \operatorname{Ec} f''^2 + A_1 \operatorname{Br} (f''(\zeta))^2 + \alpha \theta(\zeta) = 0,$$
(17)

where  $A_i$  is delineated as follows:

$$A_1 = \frac{(1 - \phi_2)^{-2.5}}{(1 - \phi_1)^{2.5}},\tag{18}$$

$$A_2 = (1 - \phi_1)(1 - \phi_2) + \phi_1(1 - \phi_2)\frac{\rho_{s_1}}{\rho_f} + \phi_2\frac{\rho_{s_2}}{\rho_f}, \quad (19)$$

$$A_{3} = \frac{\left[\sigma_{s_{1}} + 2\sigma_{f} - 2\phi_{1}(\sigma_{f} - \sigma_{s_{1}})\right] \times \left[\sigma_{s_{2}} + 2\sigma_{nf} - 2\phi_{2}(\sigma_{nf} - \sigma_{s_{2}})\right]}{\left[\sigma_{s_{1}} + 2\sigma_{f} + (\sigma_{f} - \sigma_{s_{1}})\phi_{1}\right] \times \left[\sigma_{s_{2}} + 2\sigma_{nf} + (\sigma_{nf} - \sigma_{s_{2}})\phi_{2}\right]},$$
(20)

$$A_4 = \left[ (1 - \phi_1)(1 - \phi_2) + \phi_1(1 - \phi_2) \frac{(\rho\beta)_{s_1}}{(\rho\beta)_f} \right] + \phi_2 \frac{(\rho\beta)_{s_2}}{(\rho\beta)_f}, \tag{21}$$

$$A_5 = \frac{\left[k_{s_1} + (n-1)k_f - (k_f - k_{s_1})(n-1)\phi_1\right] \times \left[k_{s_2} + (n-1)k_{nf} - (n-1)(k_{nf} - k_{s_2})\phi_2\right]}{\left[k_{s_1} + k_f(n-1) + (k_f - k_{s_1})\phi_1\right] \times \left[k_{s_2} + (n-1)k_{nf} + (k_{nf} - k_{s_2})\phi_2\right]},$$
(22)

$$A_{6} = \left\{ (1 - \phi_{2}) \left[ (1 - \phi_{1}) + \phi_{1} \frac{(\rho c_{p})_{s_{1}}}{(\rho c_{p})_{f}} \right] + \phi_{2} \frac{(\rho c_{p})_{s_{2}}}{(\rho c_{p})_{f}} \right\}. \quad (23)$$

$$Re^{\frac{1}{2}} C_{f} = A_{1} f''(0), \quad \frac{Nu}{Re^{\frac{1}{2}}} = -\left[ A_{5} + \frac{4}{3} Rd \right] \theta'(0). \quad (27)$$

### 2.6 Revised boundary conditions

The following are the related boundary conditions:

$$f(\zeta) = S, \ \lambda = f'(\zeta), \ \theta(\zeta) = 1|_{\operatorname{at} \zeta = 0},$$

$$f'(\zeta) = 0, \ \theta(\zeta) = 0|_{\operatorname{as} \zeta = \infty}$$

$$(24)$$

where  $\lambda$  is the stretching/shrinking parameter.

The governing model mentioned above represents the emerging physical parameter as follows:

$$M = \frac{\sigma_{\rm f} B_0^2}{b \rho_{\rm f}}, \ Gr = \frac{g \beta_{\rm f} (T_{\rm w} - T_{\infty}) x^3}{v_{\rm f}^2}, \ \delta = \frac{a}{b},$$

$$Re = \frac{b x^2}{v_{\rm f} (1-a t)},$$

$$\lambda^* = \frac{Gr}{Re^2}, \ Ec = \frac{u_{\rm w}^2}{c_{\rm p} (T_{\rm w} - T_{\infty})}, \ Pr = \frac{v_{\rm f}}{\alpha},$$

$$Br = \frac{\mu_{\rm f} u_{\rm w}^2}{k_{\rm f} (T_{\rm w} - T_{\infty})},$$

$$S = \frac{v_0}{\sqrt{v_{\rm f} b}}, \ Rd = \frac{4\sigma^* T_{\infty}^3}{k_{\rm f} k^*}, \ E_1 = \frac{E_0}{u_{\rm w} B_0}, \ \alpha = \frac{Q_0}{a(\rho C_{\rm p})_{\rm f}},$$

$$Ec = \frac{u_{\rm w}}{C_{\rm p} (T_{\rm w} - T_{\infty})}.$$

Coefficient of skin friction  $C_{\rm f}$ , Nusselt number Nu, tangential stress at the sheet  $\tau_{\rm w}$ , and heat flux  $q_{\rm w}$  are major considerable quantities that are referred to as:

$$q_{\rm w} = -\left[ \left( k_{\rm knf} + \frac{16\sigma^* T_{\infty}^3}{3k^*} \right) T_y \right]_{y=0}, \ \tau_{\rm w} = \mu_{\rm hnf}(u_y)_{y=0}.$$
 (26)

## 3 Physical parameters

In dimensionless form, the fascinating engineering parameters are articulated as

## 4 Entropy production

Entropy generation is a variety of industrial and technological activities that use all the energy available. As it turns out, it is essential to know how quickly a system produces entropy. Under the action of electric and magnetic phenomena, the volumetric entropy generation is given as follows:

$$S'''_{gen} = \frac{k_{hnf}}{T_{\infty}^2} (T_y)^2 + \frac{\mu_{hnf}}{T_{\infty}} (u_y)^2 + \frac{\sigma_{hnf}}{T_{\infty}} (uB - E)^2. \quad (28)$$

The above equation accounts for conduction, Joule effects, and viscosity. In non-dimensional, the entropy consequence is specified as.

$$N_{\rm G} = \frac{S'''_{\rm gen}}{S'''_{0}} = A_{5} \operatorname{Re} \theta'^{2} + A_{1} \frac{\operatorname{Br}}{\Omega} \operatorname{Re} f''^{2} + A_{3} \operatorname{Ha}^{2} \frac{\operatorname{Br}}{\Omega} (f' - E_{1})^{2},$$
(29)

### 5 Numerical scheme

The bvp4c function of the MATLAB, a commercial software, is instigated to crack the highly nonlinear system of equations. At this moment, the system of equations with a higher order is converted into a system with a lower order. Furthermore, computations in bvp4c necessitate an initial guess. The outcomes can be obtained by raising the number of steps until the requisite precision is attained, starting with an estimate at an initial mesh point. The appropriate beginning of estimation and boundary layer thickness must depend on the parametric values. Flow chart of the numerical code is obtained in Figure 2.

$$f = z_1, f' = z_2, z_3 = f'', z'_3 = f''', \theta = z_4, z_5 = \theta', \theta''$$
  
=  $z'_5$ , (30)

$$z_{3}' = -\frac{A_{2}}{A_{1}} \left[ z_{1}z_{3} - (z_{2})^{2} + \frac{\delta}{A_{1}} \left[ z_{2} + \frac{\eta}{2} z_{3} \right] \right] - \frac{A_{3}}{A_{1}} M(E_{1} - z_{2}) - \frac{A_{4}}{A_{1}} \lambda^{*} z_{4},$$
(31)

$$z_{5}' = \frac{-A_{6} \Pr\left[z_{1}z_{5} - z_{2}z_{4} - \delta\left(\frac{\eta}{2}z_{5} + 2z_{4}\right)\right] - A_{1} \operatorname{Br}(z_{3})^{2} - z_{4}\alpha - \operatorname{Ec}z_{3}^{2}}{\left[A_{5} + \frac{4}{3}\operatorname{Rd}\right]}, \quad (32)$$

$$z_1(0) = S$$
,  $z_2(0) = \lambda$ ,  $z_4(0) = 1$ , at  $\eta = 0$   
 $z_2(\infty) \to 1$ ,  $z_4(\infty) \to 0$ .  $\eta \to \infty$  (33)

Tolerance considered in this problem is  $10^{-6}$ .

The authors have opted for the aforementioned numerical approach due to several notable advantages as follows:

- 1) This method adeptly handles highly nonlinear equations.
- 2) It allows for user-adjustable error tolerance, providing flexibility in the solving process.
- 3) Complex systems of equations that are challenging to solve analytically can be effectively addressed.
- 4) Remarkably, this method offers swift solutions, significantly reducing computational time compared to other established techniques.

## 6 Discussion and results

By taking into consideration nonlinear heat source/sink, viscous dissipation, and nonlinear convection, the entropy effects of an unstable, hybrid nanofluid flow passing through a stretching/shrinking sheet are examined. The model's non-linear boundary

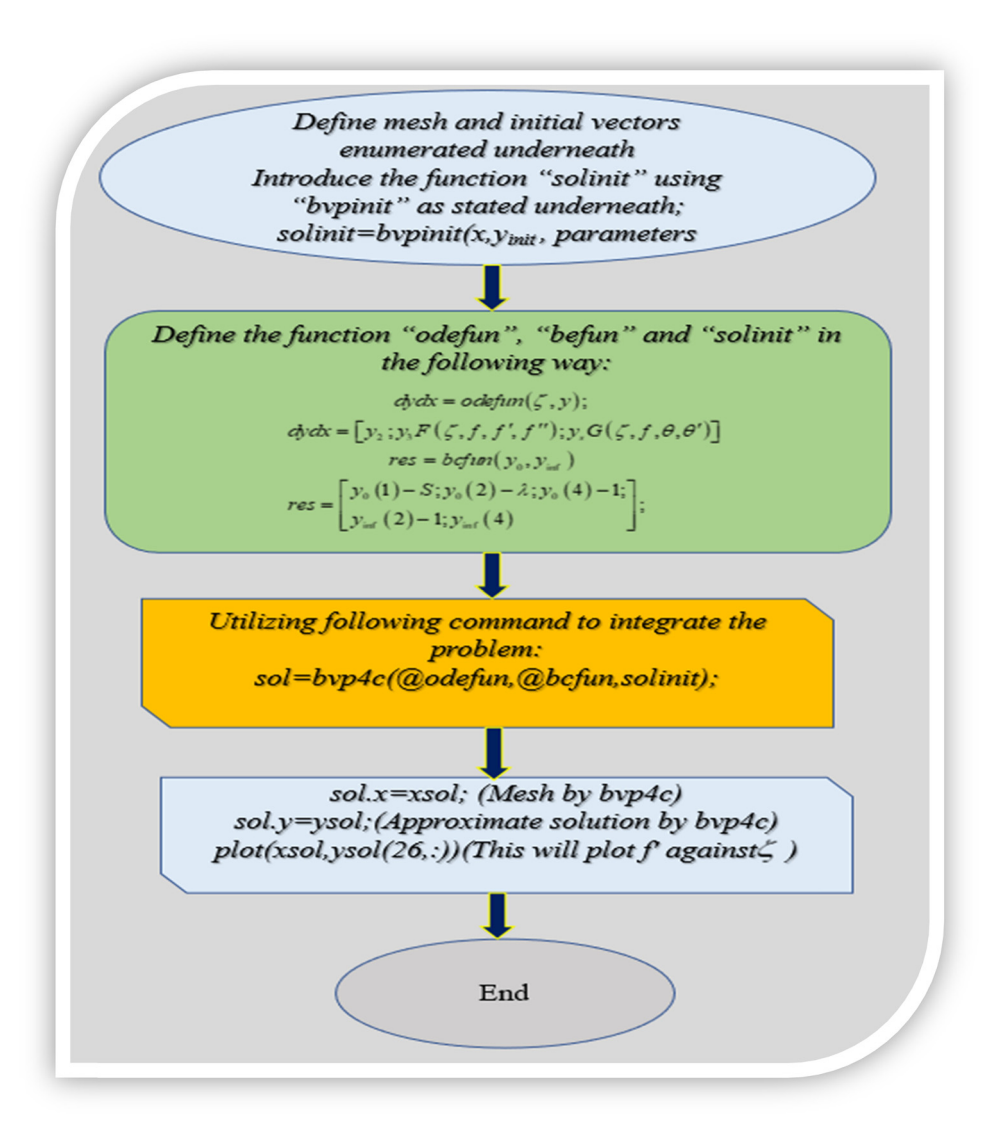
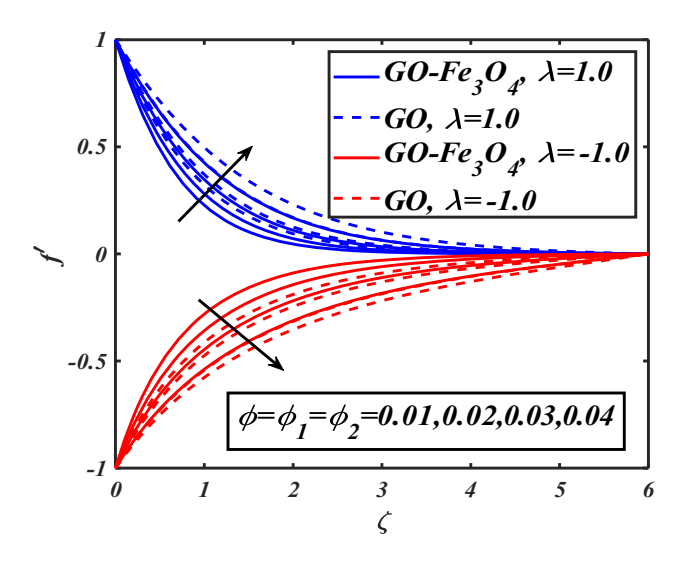


Figure 2: A flow chart of the solution process.



**Figure 3:** Evaluation of velocity distribution vs  $\phi = \phi_1 = \phi_2$ .

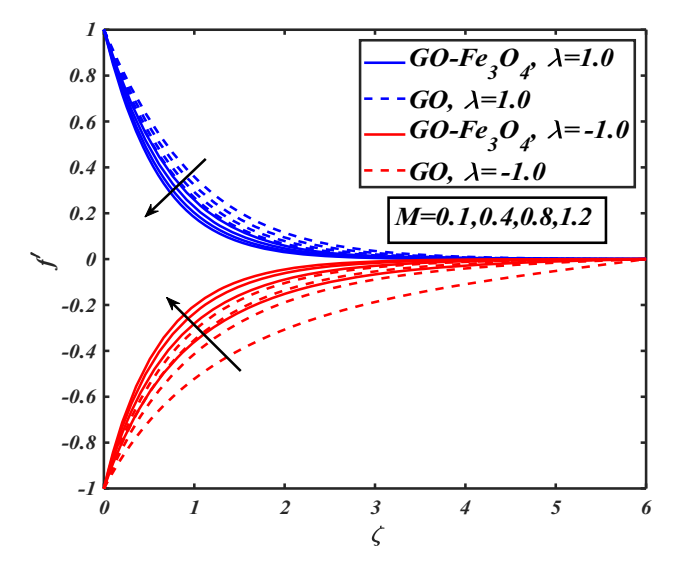
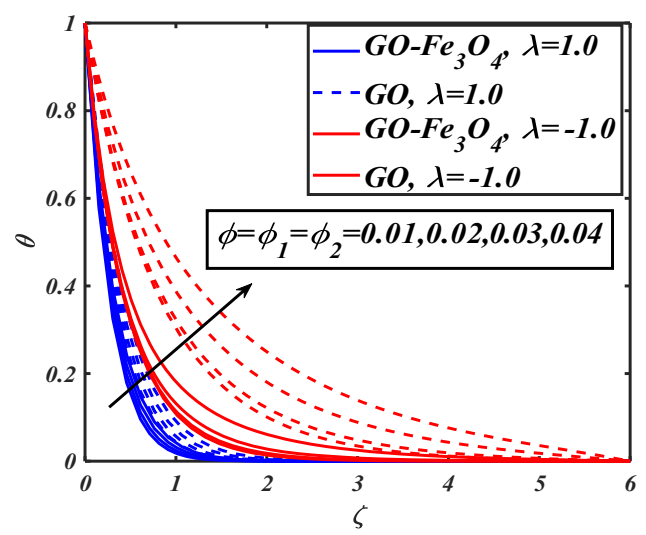


Figure 4: Evaluation of velocity distribution vs M.

value issue is solved using the bvp4c MATLAB technique. ODEs are used in this strategy to resolve the boundary value problem. The definition and explanation of the dimensionless parameterization effect on flow, temperature, Nusselt, and Sherwood numbers are the main objectives of this article. The ranges and specific values of the prominent parameter are  $0.01 \le \phi = \phi_1 = \phi_2 \le 0.04$ ,  $0.1 \le M \le 1.2$ ,  $0.1 \le \text{Rd} \le 1.2$ ,  $0.4 \le \alpha \le 1.6$ ,  $3.0 \le m \le 8.3$ ,  $5.0 \le \text{Re} \le 20.0$ , and  $-1.0 \le \lambda \le 1.0$ ,  $-0.2 \le S \le 0.2$ . We performed the process with a wide range of values for variables to evaluate the proposed algorithm's correctness. The gradual development of these variables is significantly influenced by the values of these parameters. The outcomes are visualized as streamlining, isotherm, and Nusselt number graphs. In real-world applications of the



**Figure 5:** Evaluation of temperature distribution  $vs \phi = \phi_1 = \phi_2$ .

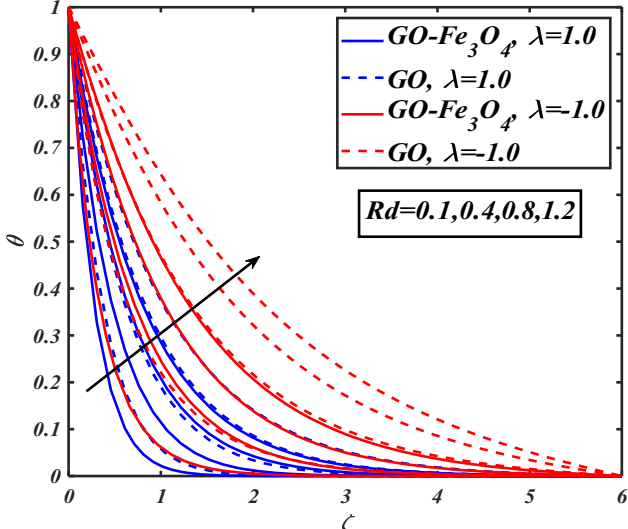


Figure 6: Evaluation of temperature distribution vs Rd.

research, using a range of values rather than specific values for the parameters might produce better results.

# 6.1 Impact of prominent parameters on the velocity profile

Figure 3 explains the aftereffects of the concentration of nanoparticles against the velocity concentration for  $GO-Fe_3O_4/H_2O$  and  $GO/H_2O$ . It can be seen that the distinct solid lines reveal the response of hybrid nanofluid and the dotted lines give the illustration of nanofluid flow with the separate stretching ( $\lambda = 1.0$ ) and shrinking ( $\lambda = -1.0$ )

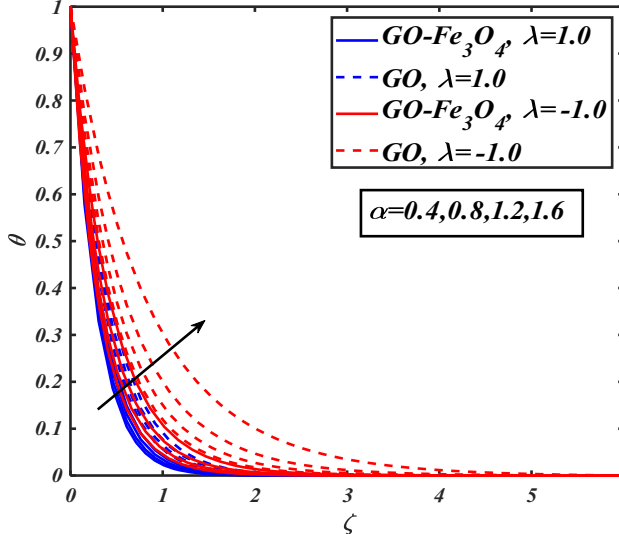
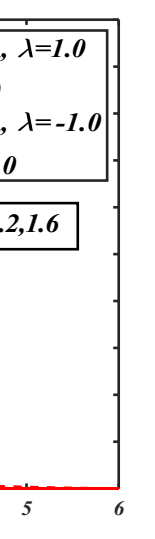


Figure 7: Evaluation of temperature distribution against heat source-sink parameter.



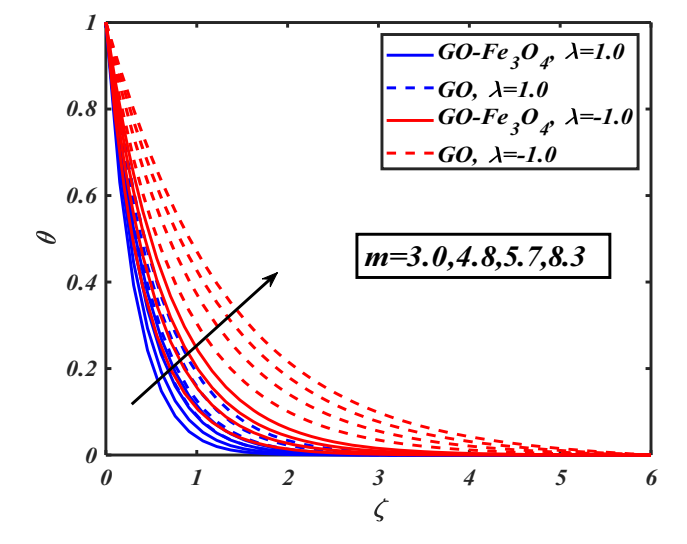
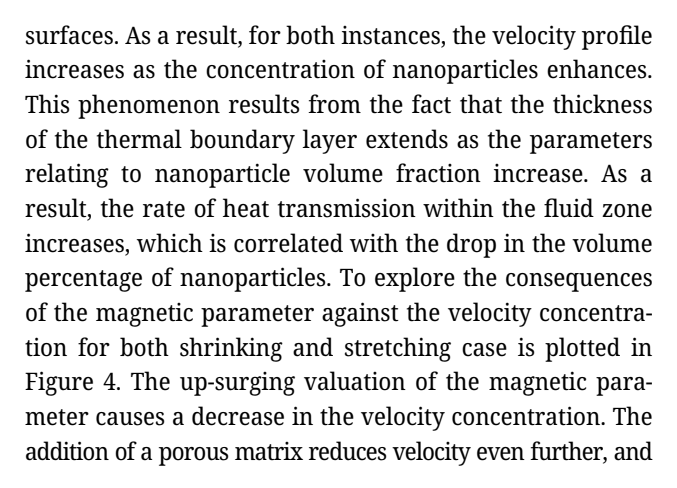


Figure 8: Evaluation of temperature distribution against shape factor m.





Nanoparticle's type	Shape	Shape factor	
Sphere		3	
Cylinder		4.8	
Platelet		5.7	
Disk		8.3	

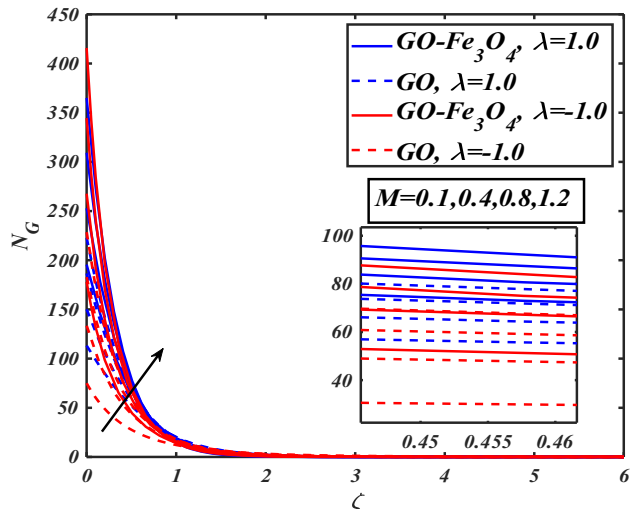
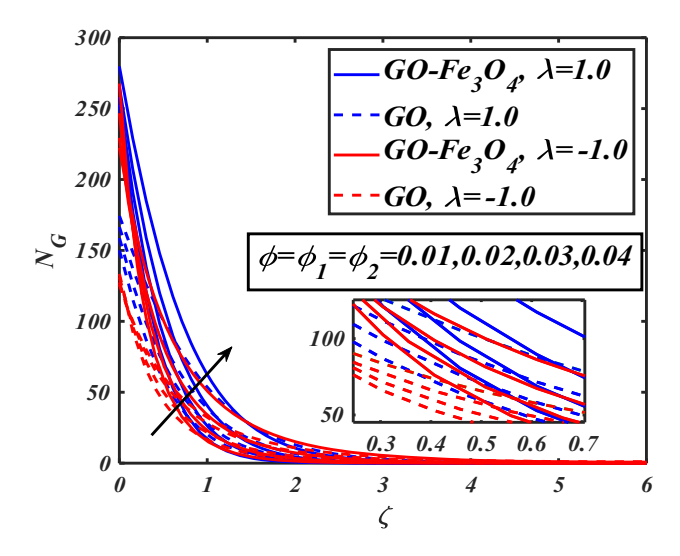


Figure 9: Evaluation of entropy generation vs M.

an increase in magnetic parameter imposes a larger Lorentz force, an electromagnetic resistive force that causes velocity to decrease. The magnetic retarding force that results from the Lorentz force raises the temperature, causing the thermal boundary layer to get thicker. On the other side, it causes the thickness of the momentum boundary layer to decrease.

## 6.2 Impact of prominent parameters on the thermal profile

Figure 5 deliberates the upshots of temperature distribution for positive values of concentration of nanoparticles.



**Figure 10:** Evaluation of entropy generation vs  $\phi = \phi_1 = \phi_2$ 

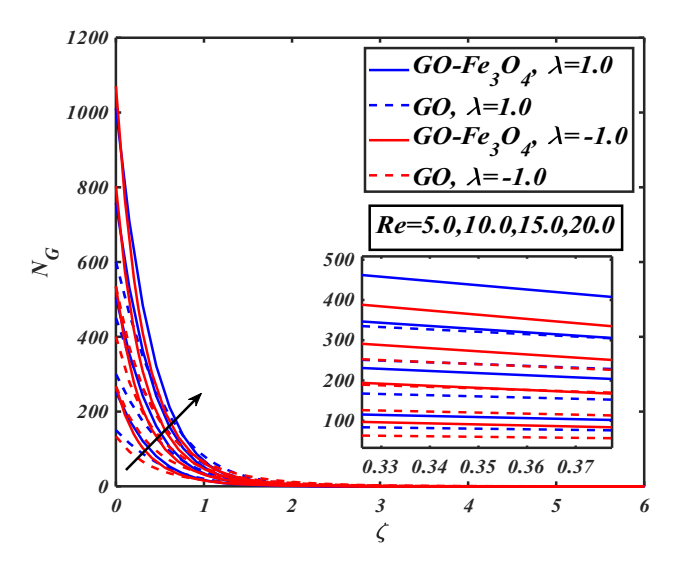
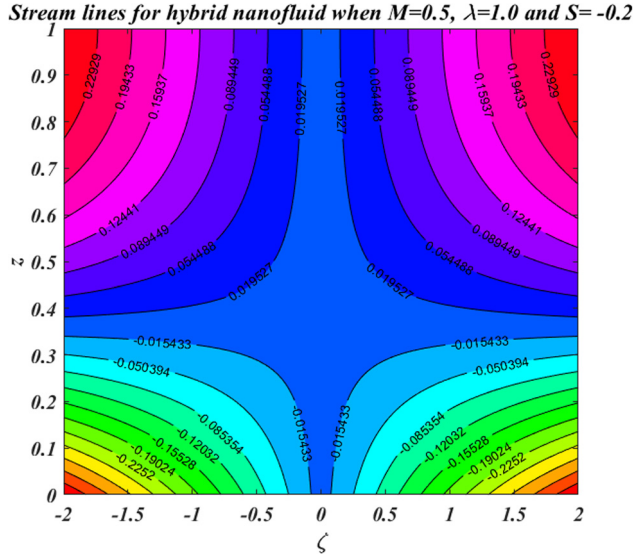
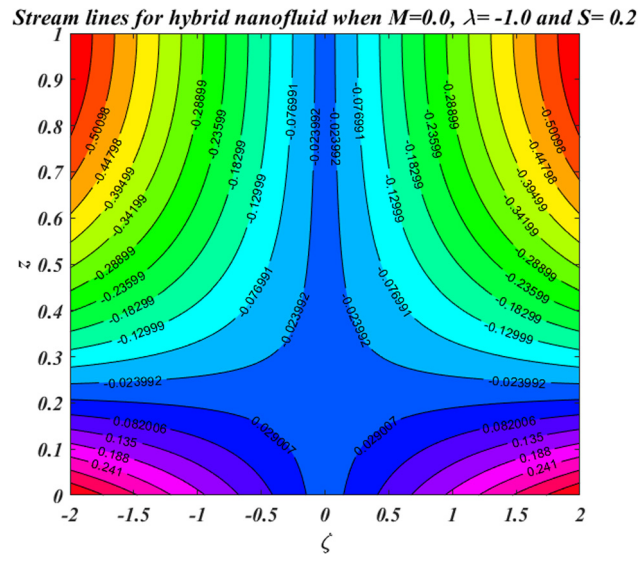


Figure 11: Evaluation of velocity distribution against Re.

For both shrinking and stretching cases, it is incurred that the temperature has an adverse impact on the growing concentration of nanoparticles. The thermal characteristics of both pure and hybrid nanofluids are significantly influenced by the volume fractions of GO and Fe<sub>3</sub>O<sub>4</sub> nanoparticles. Adding nanoparticles to base fluids has the potential to improve thermal properties in a variety of industrial settings. Nevertheless, incorporating hybrid nanocomposites into these base liquids is frequently necessary to achieve the desired heat transfer rates. Figure 6 demonstrates the impacts of thermal radiation against the temperature concentration for both shrinking/stretching cases. According to the depiction, elevating the thermal radiation parameter improved the thermal profile. The Rosseland radiative absorptivity diminishes as



**Figure 12:** Streamlines for hybrid nanofluid, when M = 0.5,  $\lambda = 1.0 \& S = 0.2$ .



**Figure 13:** Streamlines for hybrid nanofluid, when M = 0.0,  $\lambda$  = 1.0 & S = 0.2.

thermal radiation levels rise, which is the cause of this behavior. The values and rates of radiative heat transfer into the liquid therefore increase. The thickness of the thermal boundary layer increases as a result of this increased radiative heat transmission. Figure 7 reveals the features of  $\alpha$  against the temperature field for both shrinking and stretching surfaces. It is quite interesting to note that increasing variation in the heat source-sink parameter has a positive magnitude for the temperature profile. The upshots of distinct shape factors on the temperature concentration are plotted in Figure 8 (Table 2).

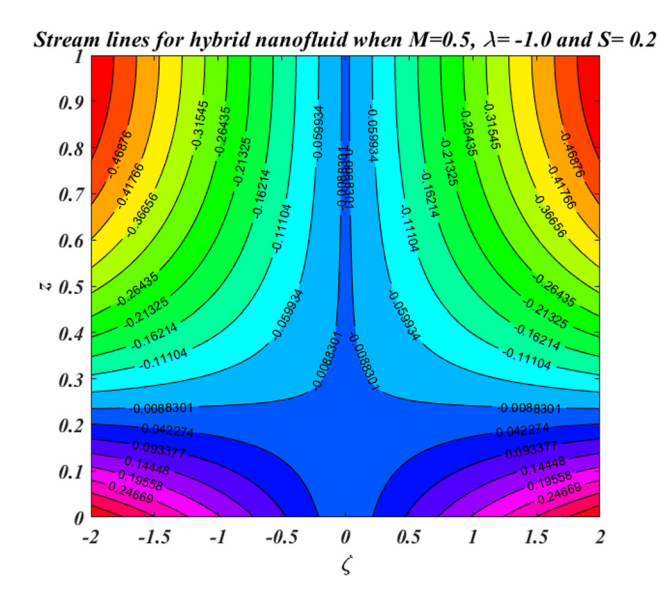


**Figure 14:** Streamlines for hybrid nanofluid, when M = 0.5,  $\lambda = 1.0 \& S = 0.2$ .

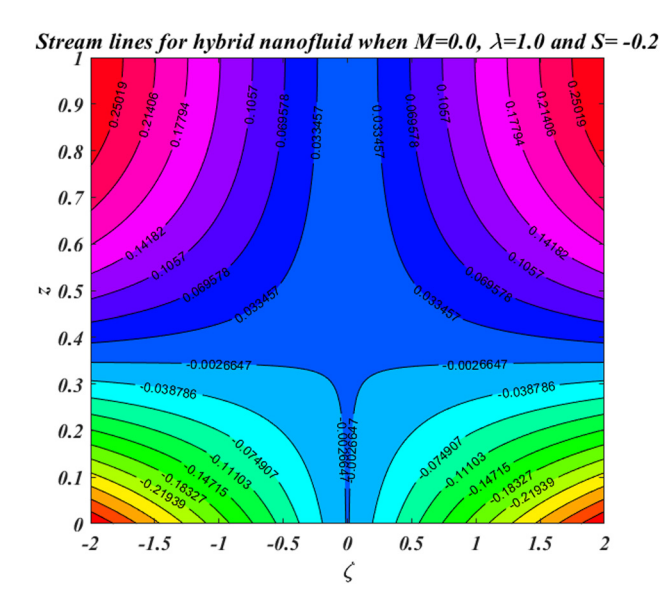


**Figure 15:** Streamlines for hybrid nanofluid, when M = 0.0,  $\lambda$  = 1.0 & S = 0.2.

The increasing values of the shape factor enhanced the temperature distribution of the fluid flow for both cases.

# 6.3 Impact of prominent parameters on entropy generation

Figure 9 is depicted to discover the marvels of magnetic parameters M for entropy generation  $N_G$  for distinct value of  $\lambda = (-1.0)\&(1.0)$ . The boosting evaluation of magnetic



Local Nusselt Number for Stretching Case of (GO-Fe<sub>2</sub>O<sub>4</sub>)

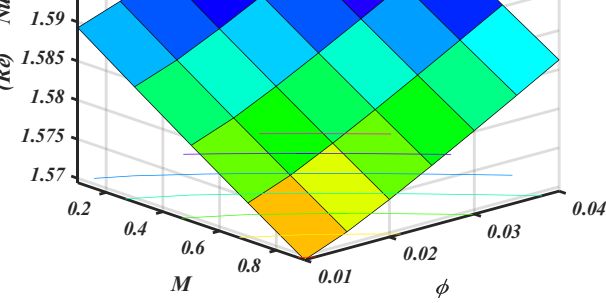


**Figure 16:** 3D plot of local Nusselt number of hybrids nanofluid for shrinking case.

**Table 3:** Numerical comparison under specific conditions, demonstrating a favorable alignment with previous studies when  $E_1=\lambda*=\phi=\phi_1=\phi_2=0, \lambda=1$ . This assessment validates the code's effectiveness in evaluating efficiency

М	δ	S	[33]	Present
0.0	0.5	0.5	1.372527	1.372527
0.5			1.479822	1.479822
1.0			1.756433	1.756432
1.5			2.127268	2.127268
2.0			2.540000	2.540000
1.2	0.0		1.831929	1.831927
	0.2		1.896669	1.896669
	0.7		1.980895	1.980895
	1.0		2.042426	2.042426
1.2	0.5	0.0	1.631209	1.631205
		0.3	1.732803	1.732803
		0.7	2.013439	2.013439
		1.5	2.199467	2.199467

Bold values represents that they are fixed for places below them until another value replace it.

parameters augmented the entropy generation for both  $GO-Fe_3O_4/H_2O$  and  $GO/H_2O$ . Figure 10 determines the impacts of concentration of nanoparticles against the entropy generation  $N_G$  of hybrid nanofluid  $GO-Fe_3O_4/H_2O$  and nanofluid  $GO/H_2O$ . Figure 11 amplifies the results of the Reynolds number Re for the entropy generation parameter  $N_G$  for both shrinking and stretching surfaces. For  $GO-Fe_3O_4/H_2O$  and  $GO/H_2O$ , it is apparent that the higher valuation of Reynolds number has a positive impact on entropy generation for hybrid nanofluid and nanofluid. The impact of the Reynolds number also contributes to the increase in entropy. The

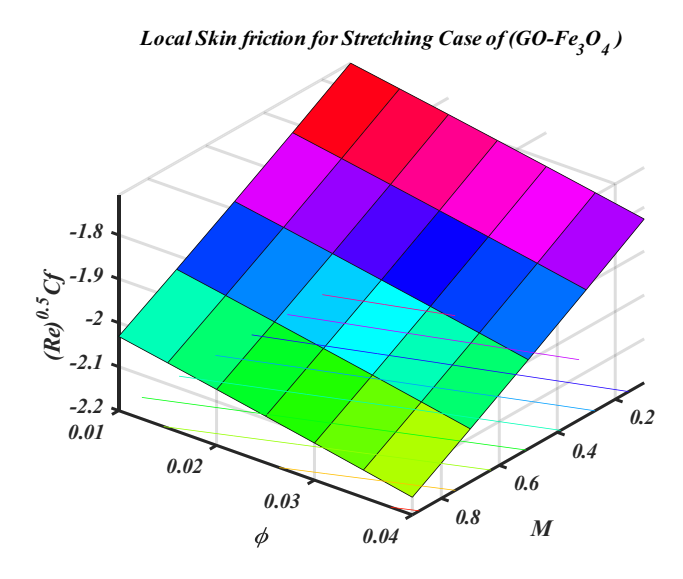


**Figure 17:** 3D plot of local skin friction of hybrid nanofluid for stretching case.

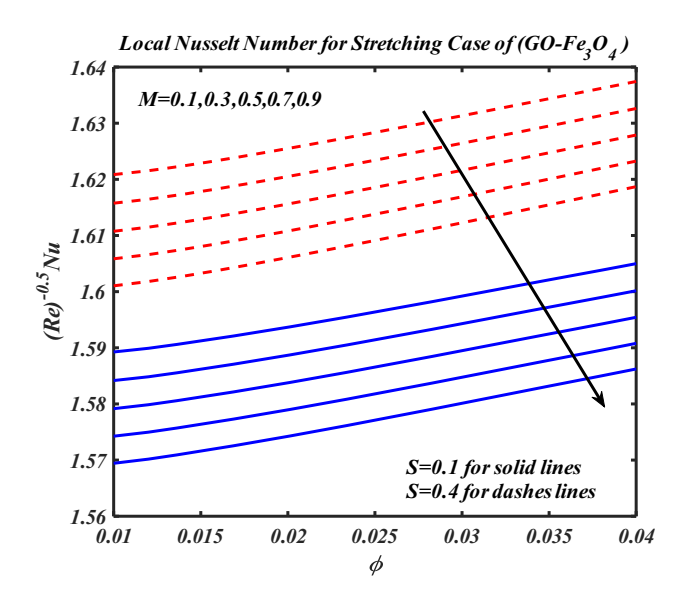


**Figure 18:** Isotherm of local Nusselt number of hybrid nanofluid against magnetic parameter for stretching case.

entropy function is heavily influenced by the Reynolds number, because the fluid moves more disturbingly as Re grows, chaotic motion occurs, and the amount of fluid friction and heat transmission to entropy formation tends to expand.

# 6.4 Conception through streamlines, isotherm, and 3D plots

Figure 12 depicts the streamlines for hybrid nanofluid with magnetic parameters M = 0.5, under suction effect S = -0.2 for stretching surface  $\lambda = 1.0$ . Figure 13 reveals

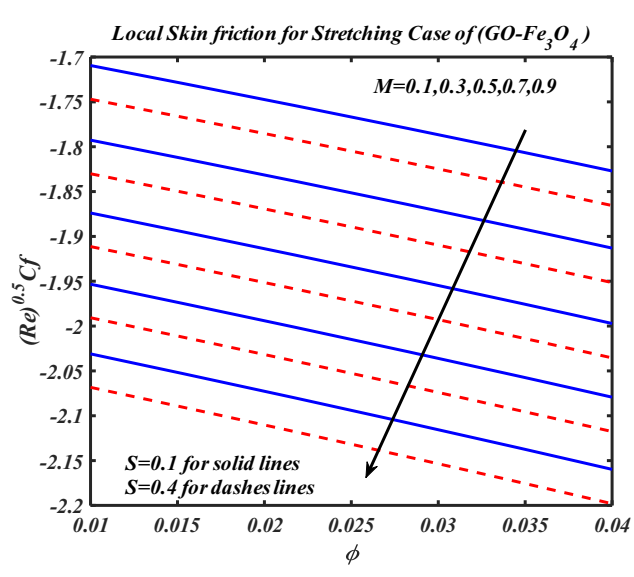


**Figure 19:** Isotherm of local skin friction of hybrid nanofluid against magnetic parameter for stretching case.

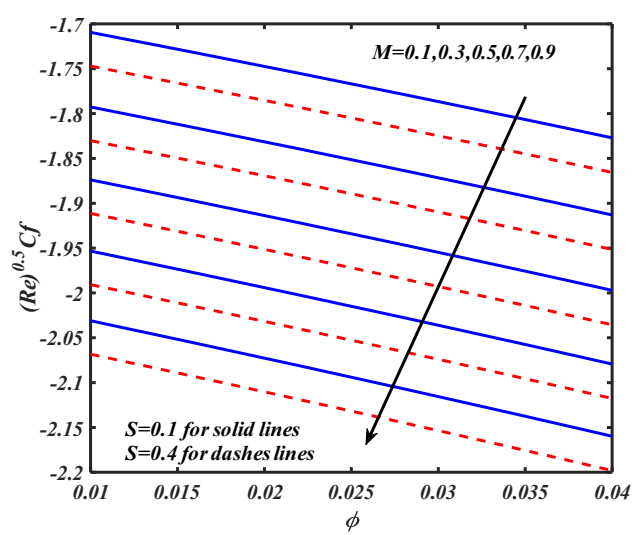


**Figure 20:** Isotherm of local skin friction of hybrid nanofluid against magnetic parameter for shrinking case.

the streamlines for a hybrid nanofluid with no magnetic impact M=0.0, under the suction S=-0.2 effect for the stretching case  $\lambda=1.0$ . Figure 14 illustrates the stream lines for hybrid nanofluid with magnetic effect M=0.5 under the influence of suction S=0.2 for shrinking surface  $\lambda=-1.0$ . Figure 15 displays the streamlines for hybrid nanofluid when no magnetic parameter is involved M=0.0 with injection S=-0.2 for stretching surface  $\lambda=1.0$ . Figure 16 discloses the 3D plot of local Nusselt number along with magnetic parameter and concentration of nanoparticles of hybrid nanofluid for stretching case  $\lambda=1.0$  (Table 3). While the effects of the other factors are barely perceptible, the

suction parameter has a substantial impact on the Nusselt number results. Figure 17 reveals the consequences of magnetic parameter and concentration of nanoparticles in the 3D plot of local skin friction of hybrid nanofluid for stretching surface. Isotherm of the local Nusselt number of hybrid nanofluid against the magnetic parameter for the stretching case is captured in Figure 18. As the concentration of the nanoparticles increase, the local Nusselt number enhances, because increase in the nanoparticles' concentration results in the thermal conductivity improvement. Also, it can be noticed that the higher number of nanoparticles increase the fluid density and decreases the fluid velocity, so the local skin friction is retorted. From the figure, it can be observed that the boosting magnetic parameter has a negative impact on the local Nusselt number for the stretching case. Figure 19 explains the outcomes of the isotherm of local skin friction for hybrid nanofluid against magnetic parameter for stretching case. Similarly, for the shrinking case, the local skin friction falls for the positive magnitude of the magnetic parameter. Figure 20 deliberated the results of isotherm of local skin friction for hybrid fluid against magnetic parameter for shrinking case. The graphical statistics demonstrate that the growing valuation of magnetic parameters reduces the local skin friction of hybrid nanofluid. It is clear from this observation that the application of surface suction significantly affects the Nusselt number and shear stress, causing them to increase. For both nanofluid situations, the suction causes a frictional interaction between fluid particles and the surface, increasing the shear rate. Notably, smaller values of the suction parameter enable optimal solutions, improving convergence and system stability. On the other hand, the effect of an applied magnetic field produces a steady decrease in the rate of heat transfer while slightly increasing the rate of shear at the surface of the sheet.

The outcomes of this investigation have numerous applications, including those in ground stream hydrology, chemical engineering, solar panel design, solar absorption and filtration systems, and solar cell technology. These findings highlight the value and adaptability of comprehending flow over a sheet in a variety of practical applications.

#### 7 Final remarks

**DE GRUYTER** 

These improved potential of hybrid nanofluids greatly boosts heat exchanger efficiency and energy savings, revolutionizing the field of thermal engineering. It enhances the heat transfer efficiency and enables controlled temperature distribution in magnetic thermal engineering applications. The forthright intention of the current declaration is to inspect the leverage of thermal radiation, heat source/sink, and suction/injection on both hybrid nanofluid Fe<sub>3</sub>O<sub>4</sub>/H<sub>2</sub>O

and nanofluid GO/H<sub>2</sub>O with shrinking/stretching surfaces. The flow panel, thermal distribution, entropy distribution, and nanoparticle concentration panel all show the physical behavior of all variables. The foremost verdicts of the ongoing study are computed below:

- · The velocity distribution boosted for concentration of nanoparticles on the other hand shows a conflicting nature of magnetic parameters for both shrinking/stretching sheets.
- The cumulative concentration of nanoparticles heightened the temperature profile against the magnetic parameter, and heat source-sink parameter.
- The variations in Reynolds number, nanoparticle concentration, and magnetic parameter positively impact the production of entropy.
- · Streamlines the hybrid nanofluid under the influence of both suction/injection for shirking/stretching surface with magnetic and no magnetic effect.
- The results are represented as streamline, isotherm, and Nusselt number plots.

We are confident that this research will help engineers and that the conclusions reached will serve as a solid basis for the design of rotating machinery, medical devices, gas turbine rotors, and thermal management systems. The paradigm of advanced heat transfer techniques frequently uses this kind of study.

**Acknowledgments:** The authors extend their appreciation to the Deanship of Scientific Research at King Khalid University, Abha, Saudi Arabia for funding this work through Large Groups Project under grant number RGP.2/536/44.

Funding information: The authors extend their appreciation to the Deanship of Scientific Research at King Khalid University, Abha, Saudi Arabia for funding this work through Large Groups Project under grant number RGP.2/536/44.

Author contributions: All authors have accepted responsibility for the entire content of this manuscript and approved its submission.

**Conflict of interest:** The authors state no conflict of interest.

#### References

Kleinstreuer C, Xu Z. Mathematical modeling and computer simulations of nanofluid flow with applications to cooling and lubrication. Fluids. 2016;1(2):16.

- [2] Choi SUS, Eastman JA. Enhancing thermal conductivity of fluids with nanoparticles. Argonne, IL (United States): Argonne National Lab. (ANL); 1995.
- [3] Esfe MH, Hajmohammad H, Toghraie D, Rostamian H, Mahian O, Wongwises S. Multi-objective optimization of nanofluid flow in double tube heat exchangers for applications in energy systems. Energy. 2017;137:160–71.
- [4] Sharma P, Said Z, Memon S, Elavarasan RM, Khalid M, Nguyen XP, et al. Comparative evaluation of AI-based intelligent GEP and ANFIS models in prediction of thermophysical properties of Fe<sub>3</sub>O<sub>4</sub>-coated MWCNT hybrid nanofluids for potential application in energy systems. Int J Energy Res. 2022;46(13):19242–57.
- [5] Mahian O, Bellos E, Markides CN, Taylor RA, Alagumalai A, Yang L, et al. Recent advances in using nanofluids in renewable energy systems and the environmental implications of their uptake. Nano Energy. 2021;86:106069.
- [6] Elsheikh AH, Sharshir SW, Mostafa ME, Essa FA, Ali MKA. Applications of nanofluids in solar energy: A review of recent advances. Renew Sustain Energy Rev. 2018;82:3483–502.
- [7] Pordanjani AH, Aghakhani S, Afrand M, Sharifpur M, Meyer JP, Xu H, et al. Nanofluids: Physical phenomena, applications in thermal systems and the environment effects – a critical review. J Clean Prod. 2021;320:128573.
- [8] Shojaie Chahregh H, Dinarvand S. TiO<sub>2</sub>-Ag/blood hybrid nanofluid flow through an artery with applications of drug delivery and blood circulation in the respiratory system. Int J Numer Methods Heat Fluid Flow. 2020;30(11):4775–96.
- [9] Saleh H, Alali E, Ebaid A. Medical applications for the flow of carbon-nanotubes suspended nanofluids in the presence of convective condition using Laplace transform. J Assoc Arab Univ Basic Appl Sci. 2017;24(1):206–12.
- [10] Ahmad S, Ali F, Khan I, Haq SU. Biomedical applications of gold nanoparticles in thermofluids flow through a porous medium. Int J Thermofluids. 2023;20:100425.
- [11] Ahmad S, Ali K, Ashraf M, Khalifa HAEW, Aziz ElSeabee FA, Tag El Din ESM. Analysis of pure nanofluid (GO/engine oil) and hybrid nanofluid (GO–Fe<sub>3</sub>O<sub>4</sub>/engine oil): Novel thermal and magnetic features. Nanotechnol Rev. 2022;11(1):2903–15.
- [12] Abu Bakar S, Md Arifin N, Khashi'ie NS, Bachok N. Hybrid nanofluid flow over a permeable shrinking sheet embedded in a porous medium with radiation and slip impacts. Mathematics. 2021;9(8):878.
- [13] Zainal NA, Nazar R, Naganthran K, Pop I. Stability analysis of MHD hybrid nanofluid flow over a stretching/shrinking sheet with quadratic velocity. Alex Eng J. 2021;60(1):915–26.
- [14] Neethu TS, Sabu AS, Mathew A, Wakif A, Areekara S. Multiple linear regression on bioconvective MHD hybrid nanofluid flow past an exponential stretching sheet with radiation and dissipation effects. Int Commun Heat Mass Transf. 2022;135:106115.
- [15] Mahesh R, Mahabaleshwar US, Kumar PNV, Öztop HF, Abu-Hamdeh N. Impact of radiation on the MHD couple stress hybrid nanofluid flow over a porous sheet with viscous dissipation. Results Eng. 2023;17:100905.
- [16] Devi SPA, Devi SSU. Numerical investigation of hydromagnetic hybrid Cu-Al<sub>2</sub>O<sub>3</sub>/water nanofluid flow over a permeable stretching sheet with suction. Int J Nonlinear Sci Numer Simul. 2016;17(5):249–57.
- [17] Venkateswarlu B, Satya Narayana PV. Cu-Al<sub>2</sub>O<sub>3</sub>/H<sub>2</sub>O hybrid nanofluid flow past a porous stretching sheet due to temperatue-

- dependent viscosity and viscous dissipation. Heat Transf. 2021:50(1):432–49.
- [18] Sajid M, Hayat T. Influence of thermal radiation on the boundary layer flow due to an exponentially stretching sheet. Int Commun Heat Mass Transf. 2008;35(3):347–56.
- [19] Zainal NA, Nazar R, Naganthran K, Pop I. MHD flow and heat transfer of hybrid nanofluid over a permeable moving surface in the presence of thermal radiation. Int J Numer Methods Heat Fluid Flow. 2021;31(3):858–79.
- [20] Sreedevi P, Sudarsana Reddy P, Chamkha A. Heat and mass transfer analysis of unsteady hybrid nanofluid flow over a stretching sheet with thermal radiation. SN Appl Sci. 2020;2(7):1222.
- [21] Mabood F, Yusuf TA, Khan WA. Cu-Al<sub>2</sub>O<sub>3</sub>-H<sub>2</sub>O hybrid nanofluid flow with melting heat transfer, irreversibility analysis and nonlinear thermal radiation. J Therm Anal Calorim. 2021;143(2):973–84.
- [22] Shatnawi TAM, Abbas N, Shatanawi W. Comparative study of Casson hybrid nanofluid models with induced magnetic radiative flow over a vertical permeable exponentially stretching sheet. AIMS Math. 2022;7(12):20545–64.
- [23] Shatnawi TAM, Abbas N, Shatanawi W. Mathematical analysis of unsteady stagnation point flow of radiative Casson hybrid nanofluid flow over a vertical Riga sheet. Mathematics. 2022;10(19):3573.
- [24] Khan MI, Alsaedi A, Hayat T, Khan NB. Modeling and computational analysis of hybrid class nanomaterials subject to entropy generation. Comput Methods Prog Biomed. 2019;179:104973.
- [25] Seth GS, Bhattacharyya A, Kumar R, Chamkha AJ. Entropy generation in hydromagnetic nanofluid flow over a non-linear stretching sheet with Navier's velocity slip and convective heat transfer. Phys Fluids. 2018;30(12):122003.
- [26] Sithole H, Mondal H, Sibanda P. Entropy generation in a second grade magnetohydrodynamic nanofluid flow over a convectively heated stretching sheet with nonlinear thermal radiation and viscous dissipation. Results Phys. 2018;9:1077–85.
- [27] Fatunmbi EO, Salawu SO. Analysis of hydromagnetic micropolar nanofluid flow past a nonlinear stretchable sheet and entropy generation with Navier slips. Int J Model Simul. 2022;42(3):359–69.
- 28] Bhatti MM, Abbas T, Rashidi MM. Entropy generation as a practical tool of optimisation for non-Newtonian nanofluid flow through a permeable stretching surface using SLM. J Comput Des Eng. 2017;4(1):21–8.
- [29] Hayat T, Yaqoob R, Qayyum S, Alsaedi A. Entropy generation optimization in nanofluid flow by variable thicked sheet. Phys A: Stat Mech its Appl. 2020;551:124022.
- [30] Tiwari RK, Das MK. Heat transfer augmentation in a two-sided liddriven differentially heated square cavity utilizing nanofluids. Int J Heat Mass Transf. 2007;50(9–10):2002–18.
- [31] Mumraiz S, Ali A, Awais M, Shutaywi M, Shah Z. Entropy generation in electrical magnetohydrodynamic flow of Al<sub>2</sub>O<sub>3</sub>-Cu/H<sub>2</sub>O hybrid nanofluid with non-uniform heat flux. J Therm Anal Calorim. 2021;143:2135–48.
- [32] Daniel YS, Aziz ZA, Ismail Z, Salah F. Entropy analysis in electrical magnetohydrodynamic (MHD) flow of nanofluid with effects of thermal radiation, viscous dissipation, and chemical reaction.

  Theor Appl Mech Lett. 2017;7(4):235–42.
- [33] Hayat T, Qasim M, Mesloub S. MHD flow and heat transfer over permeable stretching sheet with slip conditions. Int J Numer Methods Fluids. 2011;66(8):963–75.